Available online at www.sciencedirect.com
ScienceDirect
Bioelectrochemistry 69 (2006) 193 – 200
Bioelectrochemistry
www.elsevier.com/locate/bioelechem

Voltammetry and in situ scanning tunnelling microscopy of de novo designed heme protein monolayers on Au(111)-electrode surfaces

Tim Albrecht [a,b], Wen-Wu Li [c], Wolfgang Haehnel [c], Peter Hildebrandt [a], Jens Ulstrup [b,*]

[a] *Technische Universität Berlin, Institut f. Chemie, Max-Volmer Laboratorium für Biophysikalische Chemie, Straße des 17. Juni 135, D-10623 Berlin, Germany*
[b] *Technical University of Denmark (DTU), Dept. Chemistry, Nano-DTU Kemitorvet, Bldg. 207, DK-2800 Kgs. Lyngby, Denmark*
[c] *Universität Freiburg, Institut f. Biologie II (Biochemie), Schänzlestr. 1, D-79104 Freiburg, Germany*

Received 7 November 2005; accepted 21 January 2006
Available online 23 February 2006

Abstract

In the present work, we report the electrochemical characterization and in situ scanning tunnelling microscopy (STM) studies of monolayers of an artificial de novo designed heme protein MOP-C, covalently immobilized on modified Au(111) surfaces.

The protein forms closely packed monolayers, which remain electroactive upon immobilization. In situ STM images show circular structures indicating that MOP-C stands upright on the surface in accordance with the molecular design. Despite the large spatial extension of MOP-C, about 5 nm in height, conditions could be found where tip/sample interaction is minimal and proteins could be imaged without detectable tip interference.

The results indicate further that the structural sensitivity of (in situ) STM depends to a significant extent on associated electron transfer kinetics. In the present case, the heme group does not contribute significantly to the tunnelling current, apparently due to slow electron transfer kinetics. As a consequence, STM images of heme-containing and heme-free MOP-C did not reveal any notable differences in apparent height or physical extension. The apparent height of heme-containing MOP-C did not show any dependence on the substrate potential being varied around the redox potential of the protein. The mere presence of an accessible molecular energy level is not sufficient to result in detectable tunnelling current modulation.
© 2006 Elsevier B.V. All rights reserved.

Keywords: De novo design; Artificial protein; Electrochemical STM; Single-crystal electrochemistry

1. Introduction

Structural organization and functional properties of two-dimensional films of proteins, DNA-based molecules and other biomolecules adsorbed on solid supports are of broad scientific and technological interest. Focus areas include: two-dimensional adsorption patterns [1a–1c], electron transfer (ET) mechanisms of immobilized redox metalloproteins and -enzymes [1d], construction of artificial biological ET chains [1e–1g], protein/membrane interactions and drug delivery [1h, i], biologically induced corrosion and biofilms [1j,k], biocompatibility of metallic implants [1m] and analytical applications involving immobilized enzymes, antibodies and DNA-based molecular probes [1o–1q]. Most approaches to these areas have relied on macroscopic concepts and ensemble-averaged observables such as adsorption isotherms. Methods include classical surface spectroscopies, including infrared and Raman spectroscopy, ellipsometry, surface plasmon resonance spectroscopy, quartz crystal microbalance and bioelectrochemistry. The latter is here understood as interfacial electrochemical ET between metallic electrodes and adsorbed redox metalloproteins or other biological redox molecules [2,3].

Novel microscopic techniques approaching the single-molecular level of surface organization and function of biological molecules have, however, been introduced. These include, first, single-molecule fluorescence spectroscopy, single-molecule surface-enhanced resonance Raman spectroscopy (SERRS) [4] and, not in the least, the scanning probe microscopies such as atomic force (AFM) and scanning tunnelling microscopy (STM) directly in the aqueous biological media (in situ AFM and STM) [5]. Combination of in situ STM with other state-of-the-art physical electrochemistry, particularly single-crystal, well-defined electrode surfaces [6], has opened

* Corresponding author. Fax: +45 4588 3136.
E-mail address: ju@kemi.dtu.dk (J. Ulstrup).

1567-5394/$ - see front matter © 2006 Elsevier B.V. All rights reserved.
doi:10.1016/j.bioelechem.2006.01.005

new approaches to interfacial bioelectrochemistry of redox metalloproteins and metalloenzymes at the monolayer and single-molecule levels [5].

In this report, we combine voltammetry on "ultra-clean" single-crystal Au(111)-electrodes with in situ STM for the investigation of a de novo designed synthetic 4-α-helix bundle heme protein, MOP-C, immobilized on Au(111) surfaces (MOP: modular organized protein, "C" for cysteine), shown schematically in Fig. 1. The protein is composed of two different types of helices, A and B, bound alternatingly to the cysteines of the template T via maleimidopropionyl (mp) linker groups. Each helix A contains a histidine (his) residue that provides a binding site for a heme group bis-histidine coordinated in the holo MOP-C. The shielding helices B each possess a cysteine residue at the binding site opposite to the template T, which may be used to immobilize MOP-C directly on a Au(111)-surface (see, however, below) [7].

Such artificial metalloproteins or maquettes bridge the gap between natural proteins and artificial nanoscopic objects. Their secondary and tertiary structural elements can be varied systematically [8]. This facilitates approaches to new levels of metalloprotein structure-functional detail and functions have in fact been assigned to de novo designed proteins [9]. At the same time, this paves the way for efficient protein and solid surface functionalization, for example in novel types of biosensors.

The results presented extend and support previous investigations based on cyclic voltammetry, resonance Raman and surface-enhanced resonance Raman spectroscopy of MOP-C and other related MOPs [10]. They substantiate in situ STM as a powerful tool to image large (on the STM scale) protein structures, up to several nanometers, such as reported previously for natural redox metalloproteins and DNA-based molecules [11]. These observations also hold implications for intriguing and so far unsettled issues regarding the mechanism of electron tunnelling through the immobilized proteins, via the metal redox centers [11].

2. Experimental

2.1. Materials

All chemicals for electrochemistry and STM were of highest purity grade available. 9-Fluorenyl-methyloxycarbonyl (Fmoc)-protected amino acids, (2(1-*H*-benzotriazol-1-yl-1.1.3.3-tetramethyluronium)-tetrafluoroborate (TBTU), diisopropylamine (DIEA), piperidine and 5-(4-(aminomethyl)-3, 5-bis(methyloxy)phenoxy)valeric acid/polyethylene glycol/polystyrene (PAL-PEG-PS) resin were from Perseptive Biosystems. Pre-loaded Fmoc-Gly-NovaSyn TGT resin was from Nova Biochem. HPLC grade acetonitrile was from SDS. All other chemicals, including DMSO, KH_2PO_4, K_2HPO_4, K_2SO_4, cysteamine and *N*-succinimidyl-3-maleimidopropionic acid, were highest purity grade from Aldrich/Sigma or Merck.

2.2. Synthesis

The synthesis of the cyclic decapeptide serving as the template for the 4-α-helix-bundle proteins is described in detail elsewhere [12]. The Fmoc/*t*-butyl protecting group strategy was used except for the ε-NH_2 group of the C-terminal lysine and the SH group of the N-terminal cysteine which were protected by allyloxycarbonyl (alloc) and acetamidomethyl (Acm) groups, respectively. Before cleaving the peptide from the resin, the N-terminus of helix A was modified by 3-maleimidopropionic (Mp) acid for attachment to cysteines of the template [13]. The N-terminus of helix B was acetylated, the alloc group of the C-terminal lysine selectively cleaved and 3-maleimidopropionic acid coupled to the ε-NH_2 group of this lysine. The amino acid sequences for the template with alternating protecting groups of trityl (Trt) and Acm at the cysteines and the two helices with amidated C-terminus are:

Template: cyclo[C(Trt)-A-C(Acm)-P-G-C(Acm)-A-C(Trt)-P-G-]
Helix A: Mp-G-N-A-R-E-L-H-E-K-A-L-K-Q-L-E-E-L-L-K-K-W-A-NH_2
Helix B: Ac-C(Acm)-G-G-N-L-E-E-F-L-K-K-F-Q-E-A-L-E-K-A-Q-K-L-L-K(Mp)-NH_2

The helical peptides A and B were linked to the template for protein assembly [12b,13]. After selective deprotection of the Acm groups of the N-terminal cysteine, the modular protein with two free cysteines (MOP-C) was available. The helices of MOP-C are oriented in an antiparallel way such that the individual dipole moments cancel each other.

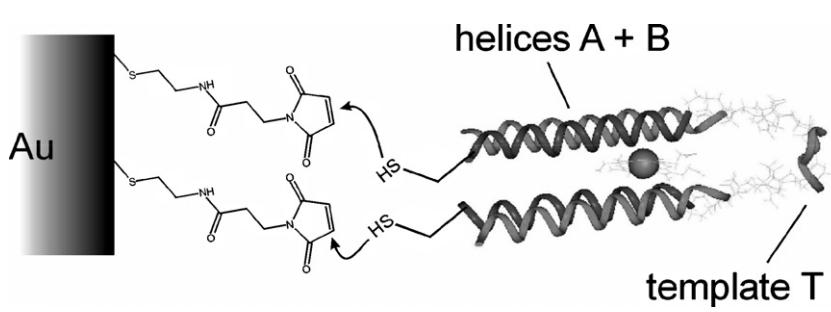

Fig. 1. Immobilization of MOP-C on a modified gold substrate; the MOP-C protein is shown to the right, with its template T and the helices A and B bound to the template in an alternating way. Only helix B contains cysteine for surface attachment and helix A histidine for heme ligation.

2.3. Mass spectrometry

Electrospray ionization (ESI) mass spectrometry of crude and purified peptides was performed on a Finnigan tandem quadrupole mass spectrometer (TSQ 700) with an electrospray interface. Horse skeletal muscle apomyoglobin with an average mass of 16,950.5 Da was used for calibration. The peptides were dissolved in 1/1 (v/v) water/methanol containing 1% acetic acid and injected directly into the electrospray interface. The mass spectra were analyzed using the programs Biomass Calculation and Biomass Deconvolution (Finnigan). The peptide mass was calculated with Pepmatch (Finnigan). The masses determined for (apo) MOP-C agree well with the calculated values (mass averages, calculated: MW_{calc} = 12,288.3 g/mol, experimental: MW_{exp} = 12,287.8 ± 0.6 g/mol).

2.4. Sample preparation

MOP-C was covalently immobilized on Au(111) electrodes involving the cysteine in helix B of MOP-C [10]. As no protein-related electrochemical response was detected upon direct immobilization, a more complex strategy with several surface modification steps was chosen which has been successful in immobilizing a related de novo protein [14]. A cysteamine monolayer was first prepared by immersing flame-annealed Au(111) electrodes in a millimolar ethanolic solution of cysteamine for 2 h. The electrodes were then rinsed with ethanol, dried in an Ar stream and transferred to a millimolar solution of *N*-succinimidyl-3-maleimidopropionic acid in dry DMSO. After 4 h, the electrodes were rinsed with pure DMSO and 10 mM potassium phosphate buffer (12.5 mM K_2SO_4), pH 7.0, and immersed in a 10 μM solution of apo MOP-C in the same buffer for 2 h. For subsequent heme incorporation, electrodes were again rinsed with buffer and dipped in 2 mM hemin/DMSO solution for 2 h. In the final step, unbound hemin was removed by rinsing the electrodes with an aqueous solution of 1% Triton X-100. The samples were then rinsed with electrolyte and transferred to the electrochemical cell containing protein- and hemin-free buffer electrolyte solution.

2.5. Electrochemistry

Au(111) bead electrodes were prepared according to Clavillier's method and characterized by sulfate adsorption patterns in 0.1 M H_2SO_4 [15]. The electrodes were annealed in a hydrogen flame prior to use, cooled in water-saturated air and then exposed to a millimolar solution of cysteamine (cf. above). Cyclic voltammetry (CV) was carried out in the hanging-meniscus configuration using an Autolab system (Eco Chemie, Netherlands). A saturated calomel electrode (SCE) served as reference electrode in all experiments except those on bare Au(111) surfaces for which a reversible hydrogen electrode (RHE) was used. The RHEs were checked vs. SCE after each experiment. All electrode potentials refer to SCE. Prior to each experiment the electrochemical cell was deoxygenated for at least 1 h using purified argon (Chrompack 5N). A gentle argon flow was maintained during all measurements. In all cases, the electrolyte solution contained 10 mM phosphate buffer, pH 7.0, and K_2SO_4 (12.5 mM) as supporting electrolyte.

2.6. In situ scanning tunneling microscopy (STM)

A PicoSPM (Molecular Imaging Co., USA) or a Rasterscope 3000 instrument (Danish Microengineering, DME A/S) with a

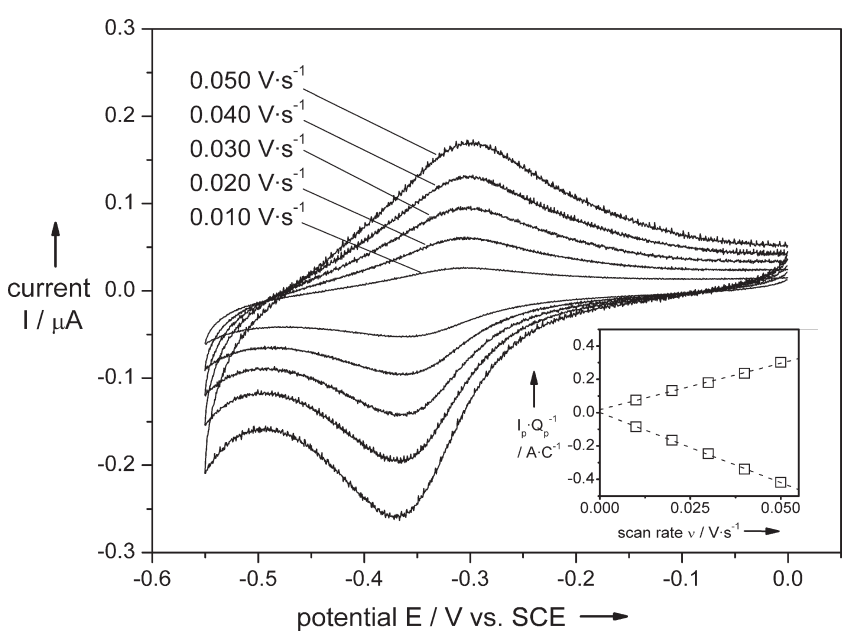

Fig. 2. Cyclic voltammograms of holo MOP-C on Au(111) at different scan rates *v*; 10 mM potassium phosphate buffer, pH 7 (12.5 mM K_2SO_4, pH 7); electrode area: 0.102 cm^2. Inset: charge-normalized peak currents as a function of scan rate *v*.

bi-potentiostatic three-electrode system were used for STM in the appropriate aqueous solutions. The in situ STM cell was in-house built. Scanner calibration was performed via the Au(111) reconstruction lines [16]. Two Pt wires served as counter and reference electrodes. A Au(111) disc (Mateck, Germany) was used as working electrode. All images were acquired in constant-current mode at room temperature. Tungsten and Pt/Ir (80:20) tips were prepared and coated as previously described [17]. Au(111) surfaces and protein samples were prepared in the same way as in electrochemical experiments. The potential of the reference electrode was calibrated vs. SCE after each experiment (E^0(Pt)=0.24±0.05 V vs. SCE at pH 7). All potentials are referred to the SCE.

3. Results and discussion

3.1. Cyclic voltammetry

Each preparation step of the protein assembly on the Au (111) surface was characterized by voltammetry [10]. No electrochemical signal could be detected in the potential range 0 to −0.55 V prior to heme incorporation. A clear signal,

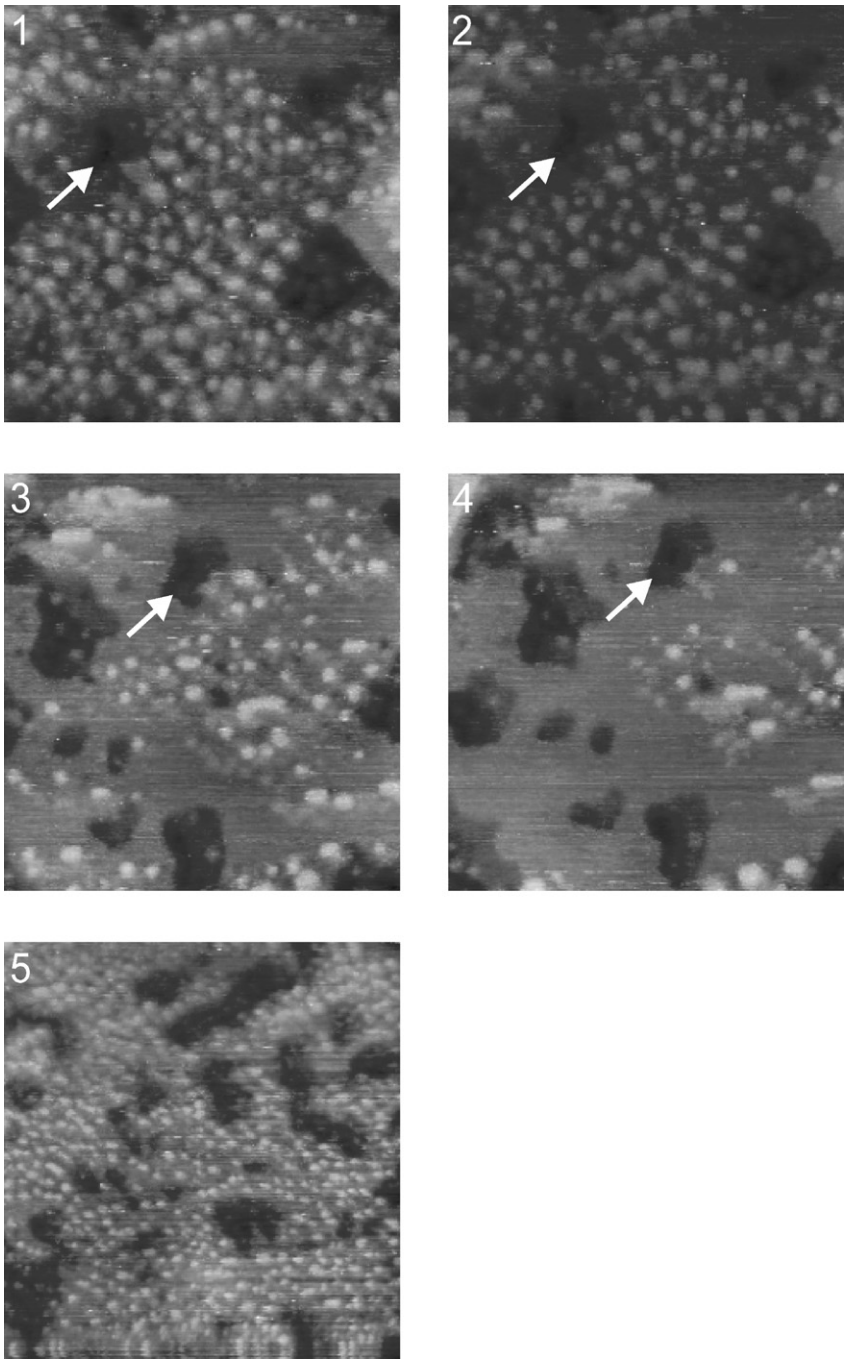

Fig. 3. In situ STM images of holo MOP-C on Au(111) in 10 mM phosphate buffer, pH 7 (12.5 mM K_2SO_4); tip: Pt/Ir (80/20); (consecutive) images 1–4: (50 nm)^2, E_s=−0.45 V, E_t=−0.25, V_{bias}=+0.2 V, I_{set}=0.45 nA; image 5: (100 nm)^2, E_s=−0.45 V, E_t=−0.25, V_{bias}=+0.2 V, I_{set}=0.4 nA; white arrow added for reference.

however, always appeared after heme incorporation (Fig. 2). The average peak potential is −0.32 V in keeping with histidine-coordinated heme [18]. The average peak charge was $2.8 \pm 1\,\mu C/cm^2$ for the first scans of each electrode, but decreased with every excursion to low potentials ($E < E^0$). This is most likely related to an oxygen-induced heme degradation process as discussed below.

The relative coverage determined from the peak area depends on the assumed protein size. A coverage of 100% is achieved with a protein base diameter of 2.7 nm, which accords with molecular modelling assuming a close-packed protein structure. Within the same modelling approach, the protein height, i.e. along its long axis, was determined to be about 5 nm. The estimated base diameter is also close to a value of 2.5 nm employed by Katz et al. for a bis-heme de novo protein of similar size [14b]. The corresponding charge for 100% relative coverage would amount to $3.3\,\mu C/cm^2$, which is slightly more than the peak charge obtained in the electrochemical experiments above.

Studies of chemically induced unfolding showed, however, that the protein does not have a closely packed "native" fold, which explains the larger size observed in the in situ STM experiments. Moreover, SERRS experiments on rough silver surfaces disclosed the existence of both bis-his coordinated low spin heme and mono-his coordinated high spin heme species in significant amounts [10]. It is not clear how far these conclusions carry over quantitatively, but a similar spin/coordination equilibrium is likely to apply for Au(111). As one MOP-C protein can bind up to two mono-his coordinated heme groups (heme/protein ratio 2:1), a high apparent electrochemical peak charge compared with the size and coverage determined by in situ STM can be understood. An additional contribution to the redox peak may arise from unspecific heme adsorption, which was, however, not found to be important on rough Ag [10]. Formation of protein multilayers is in principle possible, but a second protein layer is not likely to contribute significantly to the current as the ET rate decays rapidly with increasing distance.

The peak current normalized to the peak charge I_p/Q_p follows a linear correlation with the scan rate v. This rules out significant current contributions from diffusion. Normalization to the peak charge Q_p was needed, because, in spite of thorough deoxygenation, the redox peak and the peak current I_p decreased with the numbers of potential scans, most probably due to O_2-induced heme degradation [10,19]. Desorption of non-covalently bound protein is not likely to be the reason for the signal decay as the observed effect is highly dependent on the oxygen concentration in solution. Normalization by Q_p therefore refers directly to the number of functional protein molecules immobilized on the surface.

Overall, the voltammetric data suggest that holo MOP-C is immobilized on the Au(111) surface in an electroactive state and forms monolayers rather than multilayers.

3.2. In situ STM

Fig. 3 shows a representative image sequence of holo MOP-C on Au(111). The images show features of a thiol-modified Au(111) surface including pits. The protein MOP-C in a dense monolayer on top of the modified surface is clearly seen.

In image 1, the coverage is high and the whole surface covered by the protein. Due to tip/sample interactions, most of the protein is, however, swept away by the tip in consecutive scans (images 2–4). This shows that the surface features are indeed protein molecules and not, for example, gold islands, which could originate from thiol-induced surface etching. The Au(111) surface underneath remains unchanged (no ongoing etching process), except for a small drift indicated by the white arrow shown for reference (images 2–4). After moving to another area on the surface, the initial high coverage is observed again, substantiating that the removal of proteins is indeed a local, tip-induced effect.

The tip effect can be diminished by increasing the surface/tip distance, either by increasing the bias voltage or by reducing the setpoint (tunnelling) current. The surface area shown in Fig. 4 could be scanned repetitively with a lower setpoint current without apparent change in the image. The surface appears quite rough, presumably due to surface etching during cysteamine adsorption in the first step of protein assembly, but the dominating feature is clearly the circular-shaped protein molecules. A height profile of one of the protein molecules marked by the white arrow in Fig. 4 can be approximated by a Gaussian yielding a full-width-at-half-maximum (FWHM) of 3.9 ± 0.5 nm (Fig. 5). This is larger than comparable closely packed four-helix-bundle proteins (~3 nm), but agrees with a looser molten-globule protein structure [10]. The overall stability of holo-MOP-C towards unfolding is low compared to natural ET proteins. This would make it susceptible to destabilization at the electrochemical interface, e.g. from interfacial electric fields [20].

Some features with a length of about 7 nm (long axis) are also apparent. These may be dimeric proteins as they are too large for a single protein lying sideways, which would give approximately 5 nm. The dimers are too small to originate from intermolecular disulfide formation via their cysteines, even

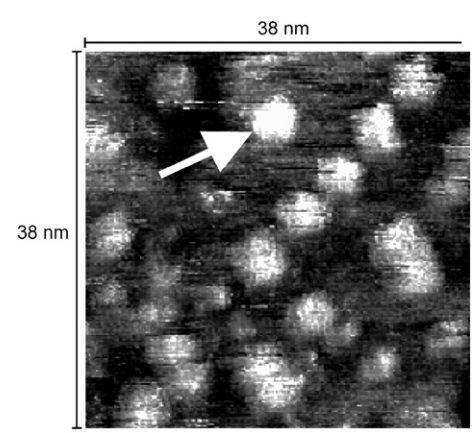

Fig. 4. In situ STM image of apo MOP-C on Au(111) in 10 mM phosphate buffer, pH 7 (12.5 mM K_2SO_4); tip: W; $E_s = -0.46$ V, $E_t = -0.24$ V, $V_{bias} = +0.22$ V, $I_{set} = 0.2$ nA; the white arrow indicates a representative protein molecule for which a height profile is shown in Fig. 5.

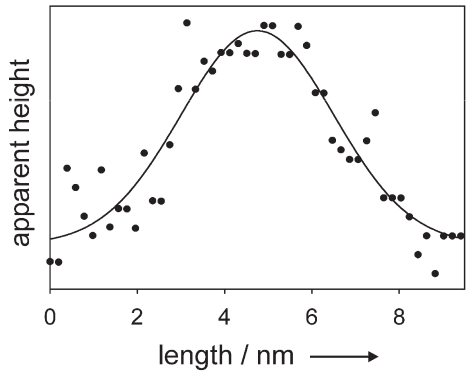

Fig. 5. Apparent height profile of the protein molecule indicated in Fig. 4 (circles), horizontal direction and Gaussian fit (solid line).

though gel filtration experiments in a similar electrolyte have disclosed about 10% dimeric structures for the heme-free protein. Strikingly, there are also signs of local ordering of the protein (Fig. 4). Protein molecules seem to line up, but no conditions could be found where the ordering extends over larger surface areas.

STM imaging experiments were, finally, undertaken both with heme-free and heme-containing protein. No significant height differences between apo- and holo-protein at the same sample potential E_s could be detected. Neither did the holo-protein show any contrast variation at different potentials around the equilibrium redox potential such as might have been expected from interfacial charge transfer theory of in situ STM processes [5].

Discrete molecular levels (such as redox centers) are known to promote electron transfer when their redox levels are tuned to resonance with the Fermi levels of the enclosing electrodes (Au (111) surface and STM tip) [21]. From condensed-matter molecular charge transfer theory, significant effects of the sample potential E_s on the STM contrast are expected, particularly in the adiabatic limit of strong electronic coupling between enclosing metal electrodes and the redox center with $eV_{bias} < \lambda$ (λ=environmental reorganization free energy) [5]. The diabatic limit of weak electronic coupling is, however, likely to apply in the present case since the heterogeneous electron transfer rate constant of ca. 10 s^{-1} is consistent with long-distance electron tunneling [10]. In contrast to the strong-coupling adiabatic limit where a single tunnelling event may include several hundreds of electrons transferred within the nuclear relaxation time τ_{rel}, only a single electron is transferred in a two-step electron transfer in the weak-coupling diabatic limit [5].

In the latter case, ET is slow ($\tau_{ET} \gg \tau_{rel}$) and requires thermal activation in both ET steps, i.e. from the substrate to the molecular level, and from the molecular level to the tip ($eV_{bias} < \lambda$). Thermal activation is again needed, before the electron can be transferred further to the tip. As a consequence, much fewer electrons are transferred within a time window τ_{rel} compared to the adiabatic limit where $\tau_{ET} \ll \tau_{rel}$. The overall enhancement of the tunnelling current is therefore smaller. The absence of detectable potential-induced variations in STM contrast for holo-MOP-C around its equilibrium redox potential and of apparent height differences between apo- and holo-protein in the STM images is also understandable from these observations. Electron transport through the redox center is simply too slow to contribute significantly to the overall tunnelling current.

4. Conclusions

The present results have shown for the first time STM images of synthetic four-helix bundle heme proteins on single-crystal Au(111) surfaces directly in aqueous buffer solution. MOP-C proteins form densely packed monolayers with features of local ordering. The immobilized proteins are electroactive, stand upright on the metal surface, and thus adopt the designed orientation. However, the in situ STM images indicate a protein size that is larger than expected for a well-folded, closely packed four-helix bundle protein, but closer to a looser, molten globule-like protein structure. There is, therefore, a need for optimizing the amino acid sequence to obtain more stable and robust protein folds, specifically in view of potential biotechnological applications as catalysts or sensors. This would also eliminate the uncertainty as to the number of heme groups (i.e. one or two) in the protein structure. Combinatorial protein de novo design as developed by one of us offers a tool to achieve these objectives in a fast and efficient way [22].

The results have demonstrated, further, that proteins of the size of MOP-C can be mapped to molecular resolution by in situ STM if the tip/surface distance is sufficiently large. While most of the protein is removed from the surface by tip/sample interaction at low bias/high setpoint current, stable images could be obtained at higher bias/lower setpoint currents. The exact position of the tip with respect to the protein layer, however, remains unknown. It cannot be ruled out that the tip actually sticks into the layer in the recorded cases, even though no protein was removed from the surface at large tip/surface distances.

The sensitivity of in situ STM to sub-molecular details is strongly related not only to the existence of accessible molecular energy levels, but also to the associated electron transfer kinetics. In the present case, ET is not fast enough to modulate single-molecular conductivities to a notable extent. In contrast, if ET processes are fast, such as in small transition metal complexes, a significant increase in tunnelling currents is observed when molecular redox levels are tuned into resonance with the Fermi levels of tip and substrate electrodes. [23].

Acknowledgements

The work was supported by the Volkswagen Foundation by the grant I/75 565 (P.H., W.H.) and by the Danish Technical Science and Research Council (J.U.). We would like to thank Dr. Jingdong Zhang for support with the STM experiments and Mr. Michael Reus for undertaking size exclusion chromatography.

References

[1] (a). T.A. Horbett, J.L. Brash (Eds.), Proteins at Interfaces: II. Fundamentals and Applications, ACS Symp. Ser., vol. 602, American Chemical Society, Washington, D.C., 1995;
(b). K. Nagayama, Protein arrays: concepts and subjects, Adv. Biophys. 34 (1997) 3–24;
(c). B. Kasemo, Biological surface science, Surf. Sci. 500 (2002) 656–677;
(d). F.A. Armstrong, G.S. Wilson, Recent developments in faradaic bioelectrochemistry, Electrochim. Acta 45 (2000) 2623–2645;
(e). G. Gilardi, A. Fantuzzi, S.J. Sadeghi, Engineering and design in the bioelectrochemistry of metalloproteins, Curr. Opin. Struct. Biol. 11 (2001) 491–499;
(f). I. Willner, E. Katz, Integration of layered redox proteins and conductive supports for bioelectronic applications, Angew. Chem., Int. Ed. 39 (2000) 1180–1219;
(g). I. Willner, B. Willner, Vectorial photoinduced electron-transfer in tailored redox-active proteins and supramolecular nanoparticle arrays, Coord. Chem. Rev. 245 (2003) 139–151;
(h). D.D. Lasic, Liposomes: From Physics to Applications, 2nd ed. Elsevier, Amsterdam, 1995;
(i). O. Mouritsen, Life as a Matter of Fat: The Emerging Science of Lipidomics, Springer, Berlin, 2005;
(j). H. Videla, Manual of Biocorrosion, CRC Press, Boca Raton, 1996;
(k). H.M. Lappin-Scott, Costerton in Microbial Biofilms, Cambridge University Press, Cambridge, 2003;
(m). D.L. Wise, V. Hasirei, K.-U. Lewandowski, M.J. Yasquemski, D.E. A. Deka, D.J. Trantolo, Biomaterials in Orthopedics, M. Dekker, New York, 2003;
(n). B.R. Eggins, Chemical Sensors and Biosensors, 2nd ed. Wiley, Chichester, 2002;
(o). L. Gorton, Biosensors and Modern Biospecific Analytical Techniques: Comprehensive Analytical Chemistry, Elsevier, Amsterdam, 2005;
(p). J. Wang, Analytical Electrochemistry, 2nd ed. Wiley, Chichester, 2000;
(q). T. Cass, Biosensors. A Practical Approach, Oxford University Press, Oxford, 2004.

[2] (a). H. Elwing, Protein absorption and ellipsometry in biomaterial research, Biomaterials 19 (1998) 397–406;
(b). Y. Maeda, H. Yamamoto, H. Kitano, Self-assembled monolayers as novel biomembrane mimetics: 1. Characterization of cytochrome-*c* bound to self-assembled monolayers on silver by surface-enhanced resonance Raman-spectroscopy, J. Phys. Chem. 99 (1995) 4837–4841;
(c). P. Tengvall, I. Lundstrom, B. Liedberg, Protein adsorption studies on model organic surfaces: an ellipsometric and infrared spectroscopic approach, Biomaterials 19 (1998) 407–422;
(d). L.M. May, D.A. Russell, The characterization of biomolecular secondary structures by surface plasmon resonance, Analyst 127 (2002) 1589–1595;
(e). K.A. Marx, Quartz crystal microbalance: a useful tool for studying thin polymer films and complex biomolecular systems at the solution–surface interface, Biomacromolecules 4 (2003) 1099–1120;
(f). C. Leger, S.J. Elliott, K.R. Hoke, L.J.C. Jeuken, A.K. Jones, F.A. Armstrong, Enzyme electrokinetics: using protein film voltammetry to investigate redox enzymes and their mechanisms, Biochemistry 42 (2003) 8653–8662.

[3] F.A. Armstrong, Insights from protein film voltammetry into mechanisms of complex biological electron-transfer reactions, J. Chem. Soc. Dalton Trans. 5 (2002) 661–671.

[4] W.E. Moerner, A dozen years of single-molecule spectroscopy in physics, chemistry, and biophysics, J. Phys. Chem., B 106 (2002) 910–927.

[5] J. Zhang, Q. Chi, A.M. Kuznetsov, A.G. Hansen, H. Wackerbarth, H.E.M. Christensen, J.E.T. Andersen, J. Ulstrup, Electronic properties of functional biomolecules at metal/aqueous interfaces, J. Phys. Chem., B 106 (2002) 1131–1152 and references therein.

[6] Q. Chi, J. Zhang, W.P. Friis, J.E.T. Andersen, J. Ulstrup, Electrochemistry of self-assembled monolayers of the blue copper protein *Pseudomonas aeruginosa* azurin on Au(111), Electrochem. Comm. 1 (1999) 91–96.

[7] A. Ihs, B. Liedberg, Chemisorption of L-cysteine and 3-mercaptopropionic acid on gold and copper surfaces—an infrared reflection absorption study, J. Colloid Interface Sci. 144 (1991) 282–292.

[8] (a). Several Contributions in Chem. Rev. 101 (10) (2001);
(b). W.F. deGrado, C.M. Summa, V. Pavone, F. Nastri, A. Lombardi, De novo design and structural characterization of proteins and metalloproteins, Annu. Rev. Biochem. 68 (1999) 779–819 and references therein.

[9] D.N. Bolon, C.A. Voigt, S.L. Mayo, De novo design of biocatalysts, Curr. Opin. Chem. Biol. 6 (2002) 125–129.

[10] T. Albrecht, W. Li, J. Ulstrup, W. Haehnel, P.G. Hildebrandt, Electrochemical and spectroscopic investigations of immobilized de novo designed heme proteins on metal electrodes, Chem. Phys. Chem. 6 (2005) 961–970.

[11] (a). E.P. Friis, J.E.T. Andersen, L.L. Madsen, P. Moller, J. Ulstrup, In situ STM and AFM of the copper protein *Pseudomonas aeruginosa* azurin, J. Electroanal. Chem. 431 (1997) 35–38;
(b). E.P. Friis, J.E.T. Andersen, Y.I. Kharkats, A.M. Kuznetsov, R.J. Nichols, J.D. Zhang, J. Ulstrup, An approach to long-range electron transfer mechanisms in metalloproteins: In situ scanning tunneling microscopy with submolecular resolution, Proc. Natl. Acad. Sci. U. S. A. 96 (1999) 1379–1384;
(c). J.D. Zhang, A.C. Welinder, A.G. Hansen, H.E.M. Christensen, J. Ulstrup, Catalytic monolayer voltammetry and in situ scanning tunnling microscopy of copper nitrite reductase on cysteamine-modified Au(111) electrodes, J. Phys. Chem., B 107 (2003) 12480–12484;
(d). J.D. Zhang, H.E.M. Christensen, B.L. Ooi, J. Ulstrup, In situ STM imaging and direct electrochemistry of *Pyrococcus furiosus* ferredoxin assembled on thiolate-modified Au(111) surfaces, Langmuir 20 (2004) 10200–10207;
(e). G.Z. Yang, L.S. Ling, L.J. Wan, X.H. Fang, C.L. Bai, Electrochemical scanning tunneling microscope imaging of self-assembled monolayer of double-stranded DNA on Au(111), J. Nanosci. Nanotechnol. 4 (2004) 561–564;
(f). J.J. Davis, H.A.O. Hill, The scanning probe microscopy of metalloproteins and metalloenzymes, Chem. Commun. 5 (2002) 393–401;
(g). P. Facci, D. Alliata, L. Andolfi, B. Schnyder, R. Kotz, Formation and characterization of protein monolayers on oxygen-exposing surfaces by multiple-step self-chemisorption, Surf. Sci. 504 (2002) 282–292.

[12] (a). M. Mutter, S. Vuilleumier, A Chemical approach to protein design—template-assembled synthetic proteins (TASP), Angew. Chem., Int. Ed. Engl. 8 (1989) 535–554;
(b). H.K. Rau, N. DeJonge, W. Haehnel, Modular synthesis of de novo designed metalloproteins for light-induced electron transfer, Proc. Natl. Acad. Sci. U. S. A. 95 (1998) 11526–11531.

[13] (a). R.H. Angeletti, L.F. Bonewald, G.B. Fields, Six-year study of peptide synthesis, Methods Enzymol. 289 (1997) 697–717;
(b). G.B. Fields, R.L. Noble, Solid-state peptide-synthesis utilizing 9-fluorenylmethoxycarbonyl amino-acids, Int. J. Pept. Protein Res. 35 (1990) 161–214;
(c). W.C. Chan, P.D. White, Fmoc Solid Phase Synthesis, Oxford University Press, 2000.

[14] (a). T. Kitagawa, T. Shimozono, T. Aikawa, T. Yoshida, H. Nishimura, Preparation and characterization of hetero-bifuntional cross-linking reagents for protein modifications, Chem. Pharm. Bull. 29 (1981) 1130–1135;
(b). E. Katz, V. Heleg-Shabtai, I. Willner, H.K. Rau, W. Haehnel, Surface reconstruction of a de novo synthesized hemoprotein for biolelectronic applications, Angew. Chem., Int. Ed. 37 (1998) 3253–3256;

(c). E. Katz, V. Heleg-Shabtai, A. Bardea, I. Willner, H.K. Rau, W. Haehnel, Fully integrated biocatalytic electrodes based on bioaffinity interactions, Biosens. Bioelectron. 13 (1998) 741–756.

[15] (a). J. Clavilier, R. Faure, G. Guinet, R. Durand, Preparation of mono-crystalline Pt microelectrodes and electrochemical study of the plane surface cut in the direction of the (111) and (110) planes, J. Electroanal. Chem. 107 (1980) 205–209;

(b). A. Hamelin, Cyclic voltammetry at gold single-crystal surfaces: 1. Behaviour at low-index faces, J. Electroanal. Chem. 411 (1996) 1–12.

[16] (a). H. Melle, E. Menzel, Superstructures on spherical gold crystals, Z. Naturforsch. 33 (1978) 282–289;

(b). K. Takayanagi, High-resolution surface study by in situ UHV transmission electron-microscopy, Ultramicroscopy 8 (1982) 145–161;

(c). U. Harten, A. Lahee, J. Toennies, Ch. Wöll, Observation of a soliton reconstruction of Au(111) by high-resolution helium-atom diffraction, Phys. Rev. Lett. 54 (1985) 2619–2622;

(d). J.V. Barth, H. Brune, G. Ertl, R.J. Behm, Scanning tunneling microscopy observations on the reconstructed Au(111) surface–atomic structure, long-range superstructure, rotational domains, and surface-defects, Phys. Rev., B 42 (1990) 9307–9318.

[17] Q. Chi, J.D. Zhang, J.U. Nielsen, E.P. Friis, I. Chorkendorff, G.W. Canters, J.E.T. Andersen, J. Ulstrup, Molecular monolayers and interfacial electron transfer of *Pseudomonas aeruginosa* azurin on Au(111), J. Am. Chem. Soc. 122 (2000) 4047–4055.

[18] (a). A. Desbois, M. Lutz, Redox control of proton transfers in membrane b-type cytochromes—an absorption and resonance Raman-study on bis(imidazole) and bis(imidazolate) model complex of iron-protoporphyrin, Eur. Biophys. J. 20 (1992) 321–335;

(b). J.M. Shifman, B.R. Gibney, R.E. Sharp, P.L. Dutton, Heme redox potential control in de novo designed four-alpha-helix bundle proteins, Biochemistry 39 (2000) 14813–14821.

[19] (a). L. Avila, H.W. Huang, C.O. Damaso, S. Lu, P. Moenne-Loccoz, M. Rivera, Coupled oxidation vs. heme oxygenation: insights from axial ligand mutants of mitochondrial cytochrome *b*(5), J. Am. Chem. Soc. 125 (2003) 4103–4110;

(b). T. Murakami, I. Morishima, T. Matsui, S. Ozaki, I. Hara, H.J. Yang, Y. Watanabe, Effects of the arrangement of a distal catalytic residue on regioselectivity and reactivity in the coupled oxidation of sperm whale myoglobin mutants, J. Am. Chem. Soc. 121 (1999) 2007–2011;

(c). M. Ihara, M. Shintaku, S. Takahashi, K. Ishimori, I. Morishima, Conversion of an electron-transfer protein into an oxygen binding protein: the axial cytochrome *b*(5) mutant with an unusually high O-2 affinity, J. Am. Chem. Soc. 122 (2000) 11535–11536.

[20] (a). D.H. Murgida, P. Hildebrandt, Heterogeneous electron-transfer of cytochrome *c* on coated silver electrodes. Electric field effects on structure and redox potential, J. Phys. Chem., B 105 (2001) 1578–1586;

(b). D.H. Murgida, P. Hildebrandt, Electrostatic-field dependent activation energies modulate electron transfer of cytochrome *c*, J. Phys. Chem., B 106 (2002) 12814–12819.

[21] (a). R.J. Hamers, D.F. Padowitz, in: D. Bonnell (Ed.), Scanning Probe Microscopy and Spectroscopy, 2nd ed., Wiley-VCH, New York, 2001, pp. 59–110;

(b). M. Kemp, A. Roitberg, V. Mujica, T. Wanta, M.A. Ratner, Molecular wires: extended coupling and disorder effects, J. Phys. Chem. 100 (1996) 8349–8355.

[22] H.K. Rau, N. DeJonge, W. Haehnel, Combinatorial synthesis of four-helix bundle hemoproteins for tuning of cofactor properties, Angew. Chem., Int. Ed. 39 (2000) 250–253.

[23] (a). T. Albrecht, A. Guckian, J. Ulstrup, J.G. Vos, Transistor-like behavior of transition metal complexes, Nano Lett. 5 (2005) 1451–1455;

(b). F. Chen, J. He, C. Nuckolls, T. Roberts, J.E. Klare, S. Lindsay, A molecular switch based on potential-induced changes of oxidation state, Nano Lett. 5 (2005) 503–506;

(c). B. Xu, X. Xiao, X. Yang, L. Zang, N. Tao, Large gate modulation in the current of a room temperature single molecule transistor, J. Am. Chem. Soc. 127 (2005) 2386–2387;

(d). A. Alessandrini, M. Gerunda, G.W. Canters, M.Ph. Verbeet, P. Facci, Electron tunnelling through azurin is mediated by the active site Cu ion, Chem. Phys. Lett. 376 (2003) 625–630;

(e). Q. Chi, O. Farver, J. Ulstrup, Long-range protein electron transfer observed at the single-molecule level: in situ mapping of redox-gated tunneling resonance, Proc. Natl. Acad. Sci. 102 (2005) 16203–16208.